Raman, photoluminescence and optical absorption studies on nanocrystalline silicon

P. Mishra*, K.P. Jain

Department of Physics, Indian Institute of Technology, Delhi, Hauz Khas, New Delhi 110016, India

Received 25 March 2002; accepted 13 May 2002

Abstract

Raman, photoluminescence (PL) and optical absorption results on silicon nanocrystals in SiO_2 matrices prepared by RF sputtering method are presented. The samples have varying Si/SiO2 compositional fraction and are annealed at different temperature and duration. The average size of the nanocrystals is determined by the lineshape analysis of the first-order Raman spectra. Raman results further indicate the existence of a threshold annealing temperature for the formation of nanocrystals and increase in the nanocrystal size with increasing temperature and duration. Size-dependent blue shift of the absorption edge is observed from absorption experiments and is supported by Raman results. Room temperature and temperature dependent PL results are analyzed with the help of a phenomenological model. The PL results in conjunction with the Raman and absorption results indicate the involvement of both the core states and the interfacial states in the luminescence process.

Keywords: Silicon nanocrystals; Quantum confinement; Raman scattering; Photoluminescence and optical absorption

1. Introduction

The experimental and theoretical study of semiconductor nanocrystallites [1-3] have generated tremendous technological and scientific interest recently, due to the unique electronic and optical properties and exhibition of new quantum phenomena. Silicon nanocrystals, especially, have been attracting much attention because of the discovery of exhibition of efficient room temperature photoluminescence (PL) and the consequent potential application in opto-electronic devices [4].

Low dimensional semiconductors are usually grown by highly sophisticated growth techniques like molecular beam epitaxy. These methods provide quasi-two dimensional structures of excellent quality. However, when the dimension is further reduced, an increasing number of difficulties arise, and although much progress was made recently, these are still less perfect until now. Quantum dots, on the other hand, are fabricated by relatively simpler methods [5-8], However, the simplicity of all these growth processes involves necessarily non-ideal sample properties such as size fluctuations, defects and surface effects due to large surface to volume ratios in small nanocrystals, etc. These factors complicate the experimental studies and despite extensive work there are still large gaps in understanding these systems.

The electronic, optical and vibrational properties of these systems are sensitive not only to the dimensions but also to the shape and other growth-related complexities such as the surface effects and size fluctuations. These properties contain information about many parameters, which are essential to the understanding of semiconductor device operation as well as the physics of the materials themselves. It is thus desirable to investigate in detail the change in electronic and vibrational properties of nanometer size structures with particular emphasis on the size and the growth conditions. Raman, PL and absorption spectroscopy are powerful non-destructive optical tools to study these changes.

The purpose of this paper is to understand the luminescence process from Si nanocrystals with emphasis on growth conditions and parameters using Raman, PL and absorption spectroscopy tools. Raman spectroscopy is utilized to ascertain the average size and crystallinity of nanocrystals. Room temperature and temperature dependent PL results have been analyzed using a phenomenological model. Above results in conjunction with absorption studies are used to explain the role of quantum confinement and interfacial states in the luminescence process from Si nanocrystals.

2. Experimental procedure

The nanocrystalline silicon samples used in this study were fabricated by co-sputtering Si and SiO2 and were annealed in argon atmosphere for various duration and at different temperature. A sputtering target consisted of 5×5 mm^2 Si pieces on a SiO2 substrate with a diameter of 8 cm and the number of Si pieces, 16, 25 and 36 were chosen to vary the Si/SiO2 compositional fraction in the sample. The target was sputtered in argon gas at 0.1 Torr with a fixed RF power of 110 W using an ANELVA FP21 RF sputtering apparatus. Sputtering time of 2 h resulted in thickness of about 3 mm. Some of the samples were annealed in argon gas of 0.3 Torr pressure at temperatures from 900 to 1000 8C for various duration.

Room temperature Raman experiment was done using a SPEX laser Raman spectrometer, an argon ion laser and photon counting electronics. The Raman spectra were recorded in 908 geometry using the 514.5 nm line of the argon ion laser. The incident power was kept low at 50 mW to avoid the laser heating of the sample. PL measurements were made using the same set-up as used for Raman. The temperature dependent PL, studies were carried out using a closed cycle refrigeration system. The samples were fixed on the cold finger of a helium cryostat using silver paste, and the temperature was regulated down to 10 K from room temperature using a HELITRON closed cycle liquid He cryostat. The cryostat was evacuated to 1×10^{-6} Torr to avoid condensation of moisture on the sample at low temperatures. A microprocessor-based digital temperature controller was used to regulate the temperature with an accuracy of 9/0.3 K. The temperature of the sample was measured accurately by mounting a chromel vs. gold thermocouple on the cold finger. An UV-VIS-NIR VARIAN spectrophotometer was used for absorption experiments.

3. Experimental results

3.1. Raman results

Figs. 1 and 2 show the first-order Raman spectra at room temperature for Si doped SiO_2 samples with 25 Si pieces on the Si sputtering target. Fig. 2(a) shows the Raman spectra of the as-deposited sample, which shows an amorphous nature with a broad hump at 470 cm^{-1} and a FWHM of 85 cm^{-1}. The sample annealed at 900 8C shows amorphous character, but the Raman spectrum shows an up-shift of 5 cm^{-1} from the peak position and narrowing by 5 cm^{-1} from the as-deposited sample. Raman peaks from other samples are found to be downshifted, broadened and asymmetric in comparison to the first-order Raman peak from crystalline silicon. It is found that with increasing annealing temperature and duration, the Raman spectrum shifts towards higher frequency, becomes narrower and is less asymmetric. Similar results are found in case of samples with different Si/SiO2 compositional fractions (16 and 36 pieces Si).

Conservation of phonon momentum q in crystalline silicon leads to a narrow zone-center optical mode at 520 cm^{-1} with a FWHM of 3.5 cm^{-1} at room temperature. In amorphous silicon, the q selection rule does not apply due to loss in long range order. All phonons, are therefore, optically allowed and the Raman spectrum resembles the phonon density of states with a broad hump at 480 cm^{-1}. Thus, the observation of this hump or sharp line at 520 cm $^{-1}$ differentiates between amorphous and crystalline silicon. In nanocrystals, the phonons are localized in small crystallites, and momentum is no longer well defined according to the uncertainty principle, thus allowing phonons with $q \neq 0$ to contribute to the Raman spectra. Thus, softening and asymmetric broadening of the first-order Raman spectra is observed. The size of the nanocrystals was estimated by fitting the Raman lineshape to the theoretically calculated lineshape from the phonon confinement model[9,10].

According to this model, the first-order Raman spectrum $I(v)$ is given by

$$I(v) = \int_q \frac{|C(0,q)|^2}{[(v - v(q))^2 + (G_0/2)^2]} dq, \quad (1)$$

where, $I(v)$ is the intensity of the Raman spectrum, $v(q)$ is the phonon dispersion of the bulk material, G_0 is the natural line-width and $C(0, q)$ is the Fourier-coefficient of the phonon confinement function.

We have chosen a Gaussian weighting function with a value of $\exp(-4\pi^2)$ at the boundary of the crystallites corresponding to a rigid confinement of the phonons in the nanocrystal (amplitude ≈ 0 at the boundary).

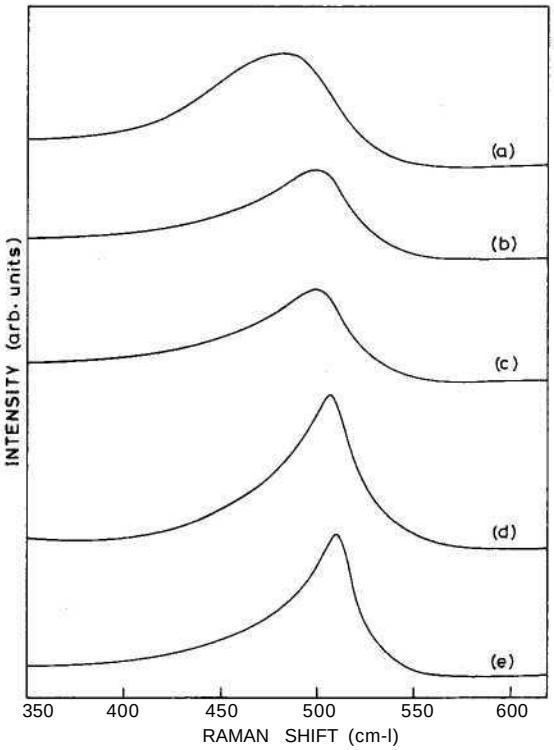

Fig. 1. First-order Raman spectra from the nanocrystalline silicon samples produced by RF sputtering with 25 Si pieces on the sputtering target and annealed in argon at temperatures (a) 900 8C, (b) 930 8C, (c) 950 8C, (d) 980 8C, (e) 1000 8C for a duration of 2 h.

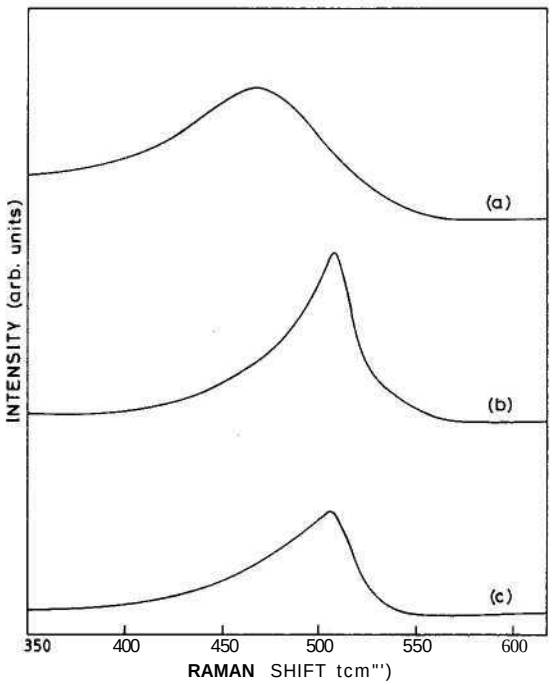

Fig. 2. First-order Raman spectra from the nanocrystalline silicon samples produced by RF sputtering with 25 Si pieces on the sputtering target (a) as deposited and annealed in argon at 1000 8C for duration of (b) 1 h (c) 30 min.

Therefore, the first-order Raman spectrum $I(v)$ is given by,

$$I(v) = \int_0^1 \frac{\exp(-q^2L^2/4a^2)}{[(co\ v\ \omega(q))^2 + (G_0=2)^2]} d^3q. \quad (2)$$

Here, q is expressed in units of $2p/a$, a is the lattice constant (5.430 Å) of silicon and G_0 is the line-width of the silicon LO phonon in C-Si bulk (~4 cm"[1] including instrumental contributions). The dispersion $v(q)$ of the LO phonon is given by the relation [11]

$$\omega^2(q) = A + B\cos(pq=2) \quad (3)$$

where A = 1.714 x 10^5 cm"[2] and B = 1.000 x 10^5 cm"[2].

The experimental line-shapes were fitted to the above model and the diameter of the crystallites is found to be in the range of 2.0-3.2 nm. Fig. 3 shows the relation between crystalline diameter vs. peak shift and broadening. Good agreement between the theory and the experiment is observed. It is observed that the average size of the nanocrystals increases for samples with higher Si/SiO_2 compositional fraction. The as-deposited samples show amorphous behavior in each case. Amorphous behavior was also observed for the samples annealed at 900 8C in all the three sets. Nanocrystalline Raman peak is observed at all other temperatures for 25 and 36 piece Si samples. For the 16 piece sample, however, we observe that the nanocrystal formation starts at an annealing temperature of 950 8C. The samples remain amorphous for an annealing temperature of 900 and 930 8C. In addition, it is observed that in all the three sets, the dimension of nanocrystals increased with increasing annealing temperature and duration.

The RF co-sputtering of Si and SiO2 leads to formation of a-SiO_x, containing non-stoichiometric amount of oxygen ($1 < x < 2$) atoms. Annealing after

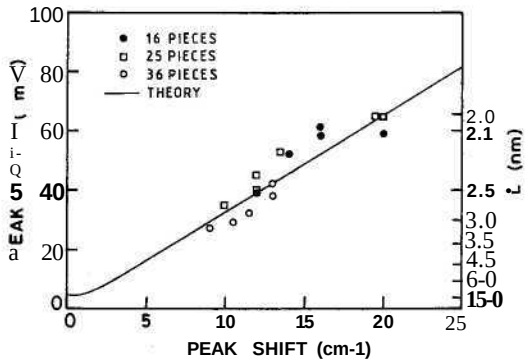

Fig. 3. Peak width vs. peak shift of the first-order Raman peak for nanocrystals with different Si/SiO_2 compositional fraction and annealed at different temperatures and durations. The solid line is theoretical curve calculated using the phonon confinement model with the Gaussian weighting function. The right ordinate shows the dimension of the nanocrystals.

deposition leads to decomposition of a-SiO_x into a two-phase state consisting of nc-Si and SiO2.

$$2SiO_2 \;0\; (2 - x)Si + xSiO_2 \quad \text{where } 0 \text{ B } x \text{ B } 2. \qquad \textbf{(4)}$$

a-SiO_x is an interesting material because it contains large amount of Si-Si bonds. A fragmented sequence of Si-Si bonds in a-SiO_x can be regarded as a silicon cluster in SiO2. Thus, a-SiO_x has the possibility of containing small Si clusters by nature. Such clusters are transferred into Si nanocrystallites under high temperature annealing. The percentage of Si is lower in case of the 16 piece sample and therefore, the size of nanocrystals is expected to be least in this case. A higher threshold temperature for the formation of nanocrystals in this case is needed because the Si clusters will be far away from each other and low annealing temperature is not sufficient for the condensation of the nanocrystals. Ma et al. [12] studied the annealing behavior of SiO_x:H films deposited by Rf PECVD process and found that Si nanocrystallite precipitation occurs after an annealing temperature of 1100 8C. Inokuma et al. [13] found that the formation of nanocrystals from SiO_x films occurred after a high temperature annealing at 1000 8C. Also, increase in size of nanocrystals with annealing temperature and duration have been confirmed by other authors [14,15].

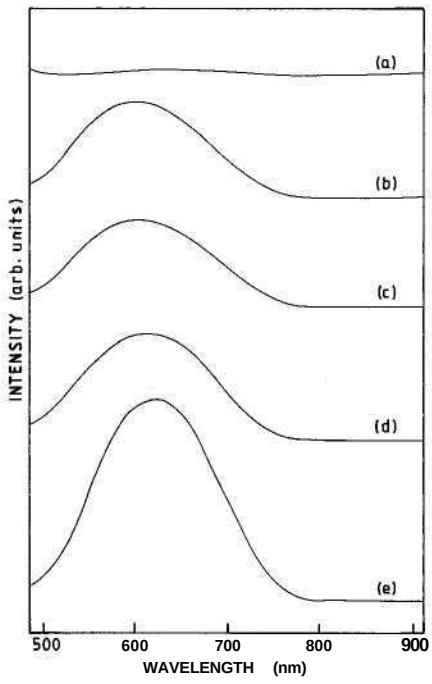

Fig. 4. Room temperature PL results from the nanocrystalline silicon samples produced by RF sputtering with 36 Si pieces on the sputtering target and annealed in argon at temperatures (a) 900 8C, (b) 930 8C, (c) 950 8C, (d) 980 8C, (e) 1000 8C for a duration of 2 h.

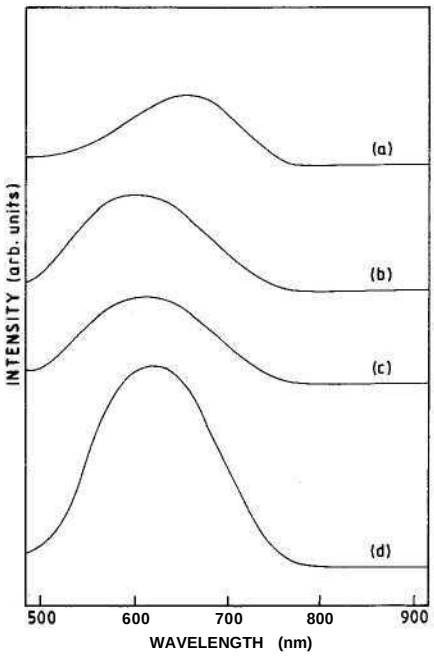

Fig. 5. Room temperature PL results from the nanocrystalline silicon samples produced by RF sputtering with 36 Si pieces on the sputtering target; (a) As deposited and annealed in argon at temperatures 1000 8C for a duration of (b) 30 min (c) 1 h (d) 2 h.

3.2. Photoluminescence results

3.2.1. Room temperature PL

Figs. 4 and 5 show the room temperature PL results from the samples with the highest Si/SiO2 compositional fraction (36 pieces Si). The PL spectrum is observed to consist of a single broad peak of FWHM 150-200 nm (300-400 meV) in the red region of the visible spectrum. PL from the sample annealed at 900 8C is found to be quite weak in intensity. The PL peak shifts monotonically to higher wavelengths and the peak intensity increases with increasing annealing temperature and duration. PL from the as-deposited sample is found to be appreciable, has a high-energy tail and is red shifted in comparison to that from other samples. Similar variation in the PL spectrum with annealing temperature and duration from the samples with 25 pieces on the SiO2 target is observed. In the samples with the 16 piece on the SiO2 target, however, the PL intensity first increases and then decreases with increasing annealing temperature and duration. In order to compare the PL spectra from the samples with different Si/SiO_2 compositional fraction, PL spectra from the as-deposited sample and the samples annealed at 980 8C for 2 h are shown in Fig. 6. It is clear that the PL peak redshifts and the intensity increases as the Si/SiO2 compositional fraction decreases, i.e. the number of Si pieces is varied from 36 to 16. Further, the PL from the samples with lowest Si/SiO_2 compositional fraction (16 pieces) resembles that from the as-deposited sample.

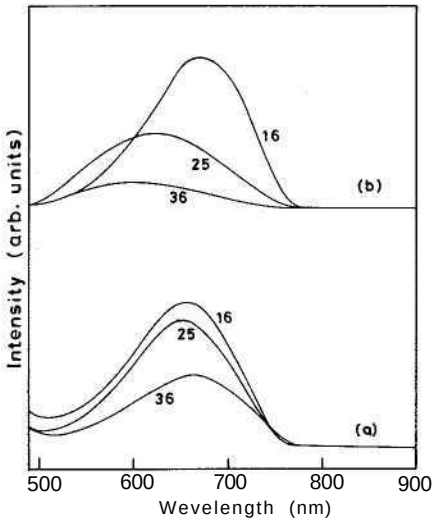

Fig. 6. A comparison of room temperature PL spectra from samples having different Si/SiO_2 compositional fraction; (a) as-deposited sample (b) annealed at 980 8C, 2 h.

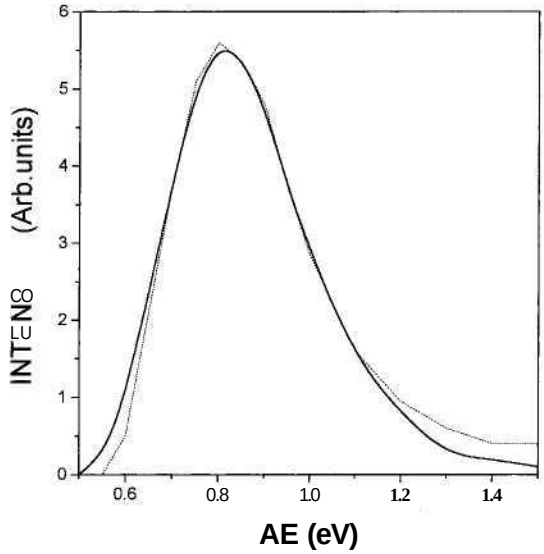

Fig. 7. The dashed curve shows the room temperature PL spectrum from the sample (16 piece) annealed at 1000 8C for 2 h. The solid line shows the theoretical fit to the experimental curve.

Quantum confinement effects have been proposed by various author [16-20] to explain the room temperature PL from Si nanocrystals. In this model, quantum confinement effects, enlarge the band gap of nanometer size clusters, increase the oscillator strength and give rise to efficient and visible luminescence. However, the confinement effect can not alone explain the broad PL spectrum in nanosilicon, which typically exhibits a FWHM of 300-400 meV. There have been suggestions that a distribution of crystallite sizes may be responsible for this, and some attempts [21-24] to model the effect of the size distribution on the PL spectrum have been made. We have used the John-Singh model [25,26] to fit our experimental PL spectra and find the average dimension of nanocrystals.

John et al. [25,26] modelled the disorder in nanosilicon by a distribution of crystallite size, calculated the shape of the consequent emission profile and explained the PL spectra from the purview of quantum confinement model. According to them, the PL lineshape is given by the expression (assuming a distribution of quantum dots)

$$P(DE) = N1\frac{1}{\Delta E^3}\exp\left[\frac{1}{2}\left(\frac{d_0}{\sigma}\right)^2\left[\left(\frac{\Delta E_0}{DE}\right)^{1/x} - 1\right]^2\right] \quad (5)$$

where N is a normalization constant, $DE = c$ (1.3 B x B 1.8) is the energy up-shift due to quantum confinement, d_0 is the mean crystallite diameter and DE_0 is the mean up-shift related to mean crystallite diameter d_0. The experimental PL spectra was fitted to the theoretical ones and could be well described by this model. Fig. 7 shows one such fit for the 16 piece sample annealed at 1000 8C, 2 h. Table 1, Table 2 and Table 3 summarize the results of the fit. The size determined from the Raman results is also shown in the tables. The size predicted by the PL lineshape fittings, is found to decrease for increasing Si/SiO2 composition, in contrast to the Raman results. However, the size determined from the PL spectrum is found to increase with increasing annealing temperature and duration in agreement with the Raman results. The as-deposited samples, which showed amorphous behavior in the Raman

Table 1
Peak energy, FWHM, average diameter *(d0)*, variance *(s)* calculated for the 16 piece Si sample from the PL lineshape fittings

Sample	PL energy (eV)	Peak d_0 (nm)	a (nm)	FWHM (meV)	Diameter (from Raman)
1000 8C, 2 h	1.82	3.05	0.42	333	2.5
980 8C, 2 h	1.86	2.95	0.41	346	2.1
950 8C, 2 h	1.87	2.82	0.47	434	2.0
930 °C, 2 h	1.92	2.65	0.49	508	Amorphous
900 8C, 2h	-	-	-	-	Amorphous
1000 8C, 1 h	1.86	2.93	0.42	367	2.3
1000 8C, 30 min	1.84	2.92	0.46	394	2.1
As-deposited	1.89	2.79	0.46	439	Amorphous

The diameter calculated from Raman lineshape analysis is also shown.

Table 2
Peak energy, FWHM, average diameter *(d0)*, variance (s) calculated for the 25 piece Si sample from the PL lineshape fittings

Sample	PL energy (eV)	Peak *d0* (nm)	*a* (nm)	FWHM (meV)	Diameter (from Raman)
1000 8C, 2 h	1.96	2.62	0.43	472	2.7
980 8C, 2 h	1.97	2.54	0.47	536	2.4
950 8C, 2 h	2.02	2.45	0.46	564	2.0
930 8C, 2 h	2.02	2.55	0.40	470	2.0
900 8C, 2h	-	-	-	-	Amorphous
1000 8C, 1 h	1.98	2.51	0.46	547	2.5
1000 8C, 30 min	2.06	2.50	0.38	467	2.2
As-deposited	1.91	2.79	0.31	390	Amorphous

The diameter calculated from Raman from lineshape analysis is also shown.

spectra, showed weak luminescence and were supposed to consist of Si dots of average diameter 2.8 nm from the PL lineshape fittings. From these results, it is clear that the Raman and PL results are un-correlated and the quantum confinement model assuming a given size distribution of nanocrystals does not seem to support the experimental results.

3.2.2. Temperature dependent PL

Fig. 8 shows the PL spectra (25 pieces, annealed at 1000 8C, 2 h) at different temperatures ranging from 25-300 K. The PL lineshape does not seem to change much with temperature variation. The variation of PL intensity and peak position are given in Fig. 9 and Fig. 10 respectively. It is noted that both the PL intensity and position show anomalous dependence with variation in temperature. The above results are analyzed again on the basis of John-Singh's model [27].

According to this model, the temperature dependence of luminescence can be analyzed in terms of competition between the radiative and the non-radiative hopping process. The radiative process shows a temperature dependence of the Arrhenius type [28]

$$R_r = \nu_r \exp\left(\frac{T_r}{T}\right) \quad (6)$$

where, T_r is a characteristic activation temperature pertaining to the radiative recombination and n_r is the characteristic frequency. The escape rate is hypothesized to have Berthlot type dependence [29,30]. Accordingly, Rhop can be written as

$$R_{hop} = \nu_B \exp\left(\frac{T}{T_B}\right) \quad (7)$$

where TB is the characteristics Berthlot temperature associated with the escape process and n_B is the characteristic frequency. The PL intensity at temperature T can be given by,

$$I(T) = \frac{I_0}{1 + n_0 \exp\left(\frac{T}{T_B} + \frac{T_r}{T}\right)} \quad (8)$$

where, $n_0 = \nu_B/\nu_r$ is the reduced frequency.

Fig. 9 shows the theoretical fittings to the experimental points of the integrated intensity vs. temperature using Eq. (8). The agreement between the theory and the experiment is found to be excellent. The characteristic Berthlot temperature T_B and the radiative temperature T_r are calculated from this fitting. The equation implies a maximum of the PL intensity at temperatures $T_m = 8]T_rT_B$. The values of T_m, T_B and T_r *are* tabulated in Table 4.

The Berthlot temperature varies between 170 and 360 K and the radiative temperature varies between 39 and 54 K. It is found that the temperature T_m corresponding to the maxima, is maximum for the 16 piece sample and minimum for the 36 piece sample. The radiative

Table 3
Peak energy, FWHM, average diameter *(d0)*, variance *(s)* calculated for the 36 piece Si sample from the PL lineshape fittings

Sample	PL energy (eV)	Peak *d0* (nm)	*a* (nm)	FWHM (meV)	Diameter (from Raman)
1000 8C, 2 h	2.02	2.51	0.42	509	3.2
980 8C, 2 h	2.00	2.51	0.45	531	3.0
950 8C, 2 h	2.01	2.46	0.46	565	2.5
930 8C, 2 h	2.02	2.48	0.44	535	2.1
900 8C, 2h	-	-	-	-	Amorphous
1000 8C, 1 h	2.01	2.45	0.45	560	2.9
1000 8C, 30 min	2.02	2.44	0.46	513	2.5
As-deposited	1.89	2.79	0.46	432	Amorphous

The diameter calculated from Raman from lineshape analysis is also shown.

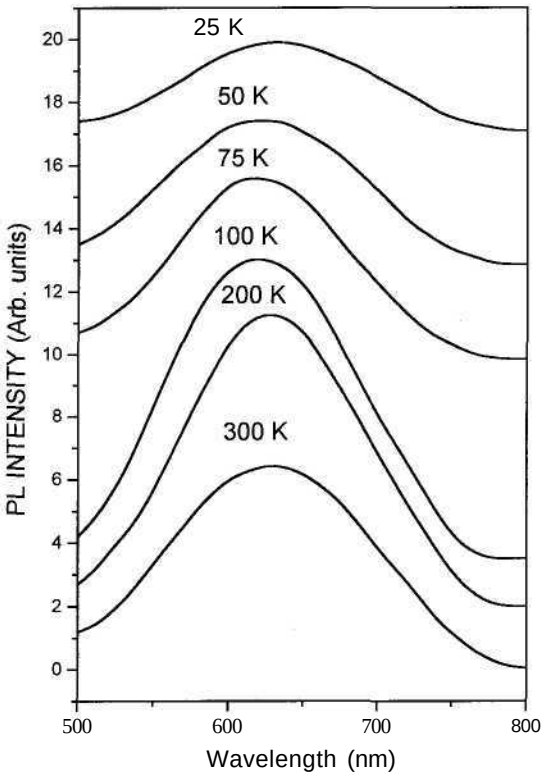

Fig. 8. Temperature dependence of the PL spectra for the samples (25 pieces) annealed at 1000 8C for 2-h duration.

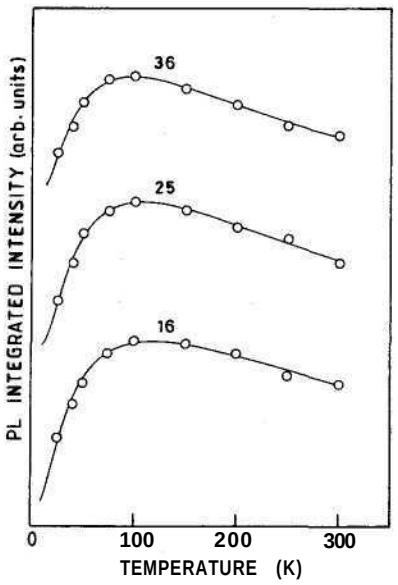

Fig. 9. Temperature dependence of integrated intensity of PL for samples having different Si/SiO_2 compositional fraction. Circles correspond to experimental points while the solid line is the theoretical fit.

temperature T_r indicates the activation energy and for our samples, the activation energy lies in the range of 3.39-4.66 meV. The activation energy can take a range of values due to inherent disorder in these materials. It is found that the activation energy increases for increasing Si/SiO_2 compositional fraction.

The Arrhenius plot of ln I_pl (logarithm of the integrated intensity of PL) for the above samples vs. 1000/T is given in Fig. 11. These plots are found to be linear for the low and high temperature part separately with different slopes. The values of the activation energy determined from the slopes of the Arrhenius plot agrees well with that from the radiative temperature T_r.

The Berthlot temperature, on the other hand, decreases for increasing Si/SiO2 composition i.e. it is maximum for the 16 piece and is minimum for the 36 piece sample. Increase in the Berthlot temperature means increase in the confinement energy of the electrons indicating reduction in the crystallite size. Thus, the samples with smaller Si/SiO_2 compositional fraction are expected to have nanocrystals of smaller dimensions.

The decrease of PL intensity at lower temperature could be due to tunneling of carriers from the crystallites to non-radiative centers [31]. This is possible due to long radiative life-time at low temperatures. The maximum in the PL intensity vs. temperature occurs at some specific temperature depending on the crystallite size. At this temperature, the radiative transitions, owing to the small activation energy are already fast enough to overwhelm the tunneling process and the thermally activated escape processes are still not important due to relatively large activation energy for the non-radiative processes. The total PL intensity is governed by the combination of radiative and non-radiative processes.

The temperature dependence of the PL peak energy is shown in Fig. 11 for the 16, 25 and 36 piece Si sample. The 25 piece Si piece Si samples showed an initial blue shift followed by a redshift, while the 16 and 36 piece Si samples showed monotonous blue shift with decreasing temperature. Bulk silicon is expected to show a monotonous blue shift with decreasing temperature at the rate of 0.19 meV K"[1] [32]. However, the shift in the PL peak position is found to be insignificant and anomalous in our samples. The anomalous temperature dependence of the PL peak position is explained on the basis of Singh-John model [33]. According to this model, the peak energy is obtained by differentiating Eq. (8) and is given by

$$hco \wedge C \;.\; - C_1 T - (C_2/T^2) \tag{9}$$

where, C_0 = £/+Eg°, U being the height of the tunneling barrier, Eg^0 is the band gap of silicon at 0 K, $C\backslash$ = 1.9 x 10^{-4} eV K^{-1}, C_2 is a constant related to the width and the frequency of the barrier.

Eq. (9) Implies a cross over of PL peak energy at T_c = $(2C_2/C_1)(^{1/3})$. Depending on the value of the cross over temperature, there can be an initial blue shift or redshift,

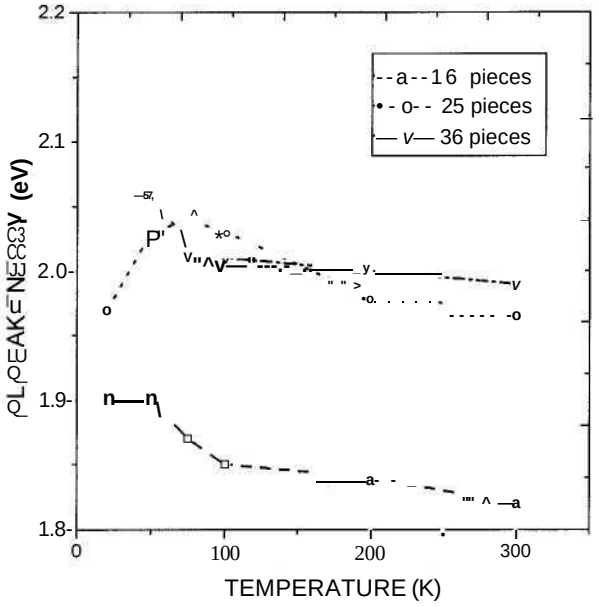

Fig. 10. Variation of the peak position of the PL spectrum with temperature, for samples having different Si/SiO_2 compositional fraction.

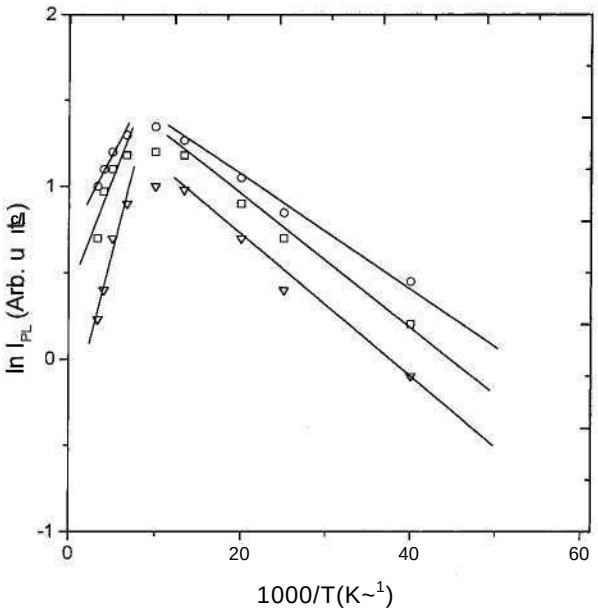

Fig. 11. Arrhenius plot showing the logarithm of the integrated intensity vs. 1000/T where T is the measured temperature. Circles, squares and the triangles correspond to 16, 25 and 36 piece samples respectively. Solid lines are straight line fits.

Table 4
The values of the temperature corresponding to maximum intensity T_m, Berthlot temperature T_B, and the radiative temperature T_r for the 16, 25 and 36 piece Si annealed at 1000 8C, 2 h

Sample (no. of Si pieces)	T_m (K)	T_B (K)	T_r (K)
16	118.3	356.1	39.3
25	107.6	243.9	47.4
36	98.1	178.24	54

Further, there could be uncertainty in the values of the barrier frequency and the width because of the inherent disorder in silicon nanocrystallites. So, the cross over temperature can lie anywhere between 20 and 2000 K. The anomalous peak energy variation of the Raman peaks can, therefore, be explained on the basis of the above model.

3.3. Optical absorption

Fig. 12 shows the spectral dependence of the absorption coefficient at 300 K for the 16, 25 and 36 piece samples annealed at 1000 8C, 2 h. It is observed that the absorption edge in the Si doped SiO2 samples is blue shifted with respect to bulk silicon. This shift increases with decreasing Si/SiO2 compositional fraction. According to the electronic structure calculations [34,35], the shift in the absorption edge is expected to be inversely proportional to the dimension of the nanocrystals. Therefore, the samples with least Si/SiO_2 compositional

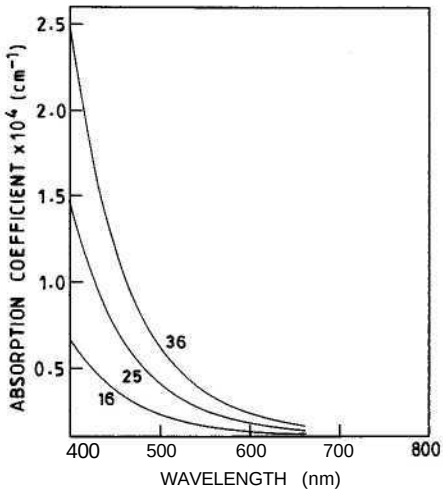

Fig. 12. Absorption spectra from the samples with different Si/SiO_2 compositional fraction and annealed at 1000 8C for 2 h.

fraction are expected to have the least size. This result is supported by the Raman results.

The absorption edge in the as-deposited sample is found to be blue shifted in comparison to the annealed sample. This is due to the presence of small Si clusters in the a-SiO_x films. Fig. 13 gives a comparative picture of the spectral dependence of the absorption coefficient of bulk silicon [36], a-Si:H [37], porous silicon [38] and the Si doped SiO_2 samples studied by us. The spectral dependence of the Si doped SiO_2 is different from that of bulk silicon over the range studied. Between 1.7 and 3.1 eV, the absorption coefficient depends exponentially on

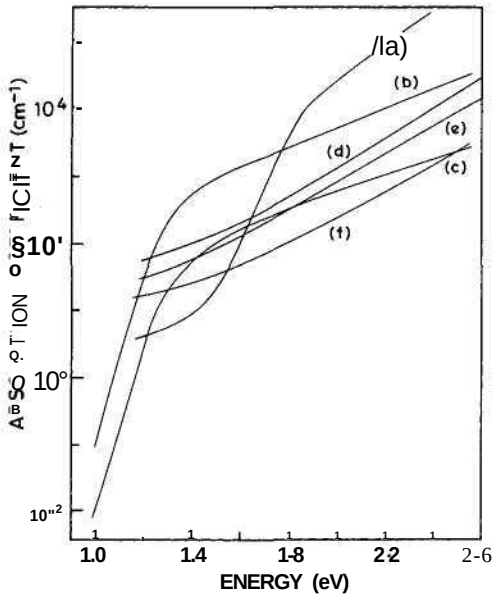

Fig. 13. Spectral dependence of the absorption coefficient of silicon in various forms (a) a-Si:H (b) bulk silicon (c) porous silicon (d) 36 pieces, annealed at 1000 8C, 2 h, (e) 25 pieces, annealed at 1000 8C, 2 h, (f) 16, pieces, annealed at 1000 8C, 2 h.

the energy. The exponential dependence of the absorption coefficient *a* in the above range resembles the Urbach tail behavior observed in the absorption of amorphous semiconductors [37]. The absorption spectrum in this range is approximately described by the relation

$$\alpha \propto \exp(E/\Gamma_\alpha) \tag{10}$$

where E is the incident energy and G_a is the characteristic Urbach energy determining the exponential slope. We fitted our results with Eq. (10), and found the exponential slope G_a for each sample. The Urbach energy G_a was found to be in the range of 250-300 meV range and was greater for samples having lower Si/SiO_2 compositional fraction. The exponential absorption tail (r_a ~ 2.50-350 meV) in nanocrystals is much larger than that of a-Si:H samples (F_a ~ 40-50 meV). This exponential behavior of the absorption coefficient has been found by many authors [39,28]. It has also been reported that porous silicon exhibits a similar behavior in the same energy range with similar values of the Urbach energy [38]. Below 1.7 eV, the absorption coefficient deviated from its exponential slope and exhibited a much gentler slope in case of the Si doped SiO_2 nanocrystals. The variation in this range resembled the behavior exhibited by an indirect semiconductor i.e. the *(ahn)12* dependence on the incident energy. Similar variations were seen in case of porous silicon [40] and Si nanocrystallites [41] prepared by other methods.

Fig. 14 shows the PL and the absorption spectra for the 16, 25 and 36 Si pieces annealed at 1000 8C, 2 h respectively. Although the value of absorption coefficient may not be exact because of discrepancy in values of *R* (reflection coefficient), but there are some points which are quite clear. The absorption in the films rises sharply for these samples at energies higher than the peak in the PL spectrum. The samples showing a greater absorption edge shift from the bulk position exhibit PL, at smaller energy. In other words, the Stoke's shift between absorption and PL is highest in case of samples having least S/SiO_2 compositional fraction (i.e. 16 pieces).

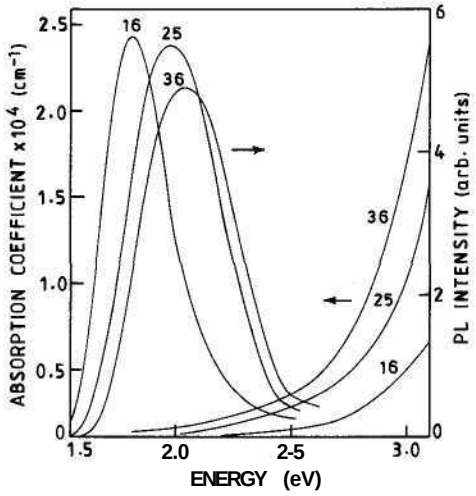

Fig. 14. PL and absorption spectra for the samples with different Si/SiO_2 compositional fraction and annealed at 1000 8C, 2 h.

4. Discussion

Apparently, the quantum confinement effects do not seem to explain the above experimental results to full extent. According to the pure confinement model, confinement of carriers in the nm size crystallites enhance the band gap and the oscillator strength of optical transitions and thus we obtain efficient PL in the visible region. The band gap of nanocrystallites depend inversely on the square of the dimension according to the effective mass theory [20]. Therefore, the PL peak energies and the shift in the absorption threshold should increase with the decrease in the dimension of nanocrystals. Raman as well as the absorption results suggested that the dimensions of nanocrystals increase with the increase in the Si/SiO_2 compositional fraction. However, the analysis of the PL lineshape showed that the dimensions decreased with increasing Si/SiO_2 composition. Also, the samples, which showed amorphous nature in the Raman, exhibited weak luminescence and had the absorption edge more blue shifted than the annealed ones. The large Urbach energy is also unexplained on the basis of the pure confinement model.

Several authors have proposed the concept of localized surface states in the process of luminescence

[42,43]. These models predict that large number of surface states are present in Si nanocrystallites because of large surface to volume ratio. In these models, the absorption process is mainly governed by the crystalline core and the carriers are transferred to the surface states where they recombine radiatively. The broad PL is explained on the basis of the inhomogeneities of the sample such as the size distribution and the consequent fluctuation of the surface potentials. Kanemitsu et al. [6,39] proposed a three-region interface model, according to which the excitons are confined in a spherical shell, an interfacial layer between the C-Si core and the a-SiO_2 layer, and the exciton confinement in the interfacial layer increases the oscillator strength and the PL intensity. The absorption process is assumed to be governed by the crystallite core.

On the basis of our results, we think that the quantum confinement effects do govern the absorption process. However, for the PL process, the surface effects can not be neglected and it is understood that they play an important role in the luminescence process. The blue shift of the absorption edge with decreasing dimensions in our samples indicates that quantum confinement effects do enhance the band gap. Higher blue shift of the absorption edge in the as-deposited sample than the annealed samples is a result of the presence of a large number of Si clusters in the a-SiO_x matrix. Annealing causes precipitation of larger nanocrystallites and consequently, the band gap decreases. The large Urbach energy in the absorption process is understood in terms of the nanoscopic disorder of the nanocrystallites, such as variation in the size and shape of nanocrystals, surface conditions and variations in the surface roughness and structure.

On the other hand, the analysis of the process of PL is rather complicated. The PL line-shapes in our samples can be explained satisfactorily within the framework of John-Singh model. The temperature dependence of the PL process could also be understood on the basis of this model. However, the PL results showed disagreement with both the Raman and the absorption results. Therefore, we suggest that the PL process is governed by recombinations in both the core and the interface. According to the three-region interface model proposed by Kanemitsu et al. [6], the interface layer between the Si core and the SiO_2 layer possesses a direct band gap between 1.7 and 2 eV depending on the O_2, covering ratio between 100 and 20%. The size of nanocrystals calculated from our Raman results lies in the range of 2.0-3.2 nm, which corresponds to an increased band gap of the core in the range of 1.85-2.7 eV according to the electronic structure calculations [34]. The excited carriers therefore, recombine radiatively either in the core or in the interfacial layer depending on the relative band gaps. The samples having the least Si/SiO_2 compositional fraction (16 pieces Si), have nanocrystals of smallest dimensions (determined from Raman experiments), and are expected to have band gap around 2.7 eV. However, for this compositional fraction, the O_2 covering ratio is also expected to be maximum and thus the band gap of the interface layer is expected to be minimum. Therefore, the dominant recombination process in this case will be interface based. This also explains the identical but weak luminescence from the as-deposited samples, which contain a small number of Si clusters. The small Si clusters have band gap higher than the annealed ones (confirmed from the absorption experiments), and the recombination in this case is mostly interface related. With the increase in the Si/SiO_2 compositional fraction, the average size of nanocrystals increases thus decreasing the band gap of the core, but the O_2 covering ratio also decreases leading to an enhanced band gap of the interface. This leads to a predominant core related recombination.

The increase in the intensity of the PL with decreasing Si/SiO_2 compositional fraction can be explained on the basis of more efficient confinement of excitons in the interface due to large difference in band gaps of the core and the interface. The PL intensity variation with annealing time and temperature depends on the number of nanocrystallites precipitated from SiO_x, and the final nanocrystal size distribution. Negligible luminescence from the samples annealed at 900 8C indicates the formation of large number of non-radiative recombination centers at low temperature annealing. The temperature dependent PL results were explained satisfactorily on the basis of a competition between radiative and non-radiative processes. In the light of the interface and the quantum confinement model, this explanation can still hold good, where the carriers may recombine radiatively either in the core or the interface or may tunnel through the SiO_2 matrix and recombine non-radiatively there. Storage of the samples in ambient air led to a two-peak behavior and degradation of the intensity of the PL spectrum, thus further supporting the involvement of the localized surface states in the PL process in the Si doped SiO_2 samples.

5. Conclusion

Raman, PL and optical absorption results on Si nanocrystals in SiO_2 matrices having different Si/SiO_2 compositional fraction and annealed at different temperature and duration are analyzed. The average size of nanocrystals is obtained by an analysis of the first-order Raman lineshape and is found to be in the range of 2-3.2 nm. Raman results also indicate a threshold annealing temperature for the formation of nanocrystals. The average size of nanocrystals is found to increase with increasing Si/SiO_2 compositional fraction and increasing annealing temperature and duration. The results are

understood in terms of the precipitation of Si nanocrystals and SiO_2 in the annealing process from a-SiO_x (1 B *x* B/2).

PL spectra from these samples were in the red region with FWHM from 300 to 400 meV range and were analyzed by a phenomenological model. The average diameter was estimated to be in the range of 2.4-3 nm and found to be higher for samples with lower Si/SiO2 compositional fraction as opposed to the Raman results. The temperature dependence of the PL intensity and peak position is explained on the basis of a competition between radiative and non-radiative processes.

The absorption edge in the silicon nanocrystal samples is found to be blue shifted in comparison to the bulk silicon. The blue shift of the absorption edge was found to be increasing for decreasing Si/SiO_2 compositional fraction. This result is in conformity with Raman result predicting a smaller size far smaller Si/SiO2 compositional fraction and consequently, a large shift in the band edge.

The above results are analyzed in terms of the involvement of the crystalline core and the interfacial layer between Si nanocrystals and SiO_2 containing non-stoichiometric amount of oxygen atoms and possessing a direct band gap in the range of 1.7-2.0 eV depending on the O_2 covering ratio. The band gap of the core is between 1.7 and 2.7 eV according to the size calculated from the Raman results and the electronic structure calculations. The absorption process is governed by the crystalline core while the PL process occurs via either the core or the interface depending on the relative band gaps. For the samples with the least Si/SiO2 compositional fraction, the major contribution to the PL is from the interfacial layer, since the O2 covering ratio is maximum leading to a lower band gap and the size of the nanocrystals is minimum leading to a higher core band gap. In the samples with higher Si/SiO_2 compositional fraction, the radiative recombination inside the core dominates due to reversal of the conditions. The intensity and peak shift variation of the PL with annealing temperature and duration is due to contribution of several factors such as the change in the dimension of nanocrystals, O_2 covering ratio and the amount of SiO_x and the consequent variation of the oscillator strengths of optical transitions. The extra sensitivity of the PL shape, position and intensity to atmospheric storage further confirms the involvement of the surface localized states in the luminescence process.

Acknowledgements

The authors would like to thank Prof. Shinji Nozaki, University of Electro-Communications, Tokyo for providing the silicon nanocrystal samples used in the above study.

References

[1] F. Henneberger, S. Schmitt-Rink, E.O. Gabel, Optics of Semiconductor Nanostructures, Academic Verlag, Berlin, 1993.
[2] M. Read, W. Kirk (Eds.), Nanostructures and Mesoscopic Systems, Academic Verlag, San Diego, 1991.
[3] P. Mishra, K.P. Jain, Phys. Rev. B 62 (2000) 14790.
[4] D.J. Lockwood (Ed.), Light Emission in Silicon from Physics to Devices, Semiconductor and Semimetals, vol. 49, Academic Press, New York, 1998.
[5] R.E. Hummel, A. Morrone, M. Ludwig, S.S. Chang, Appl. Phys. Lett. 63 (1993) 2771.
[6] Y. Kanemitsu, T. Ogawa, K. Shiraishi, K. Takeda, Phys. Rev. B 48 (1993) 4883.
[7] Y. Osaka, K. Tsunetomo, F. Toyomura, H. Myoren, K. Kohno, Jpn J. Appl. Phys. 31 (Part 2) (1992) L365.
[8] P. Mishra, K.P. Jain, Phys. Rev. B 64 (2001) 073304.
[9] H. Richter, Z.P. Wang, L. Ley, Solid State Commun. 39 (1981) 625.
[10] I.H. Campbell, P.M. Fauchet, Solid State Commun. 58 (1986) 739.
[11] Y. Kanemitsu, H. Uto, Y. Masumoto, T. Matsumoto, T. Futagi, H. Mimura, Phys. Rev. B 48 (1993) 2827.
[12] Z.-X. Ma, X.-B. Liao, J. He, W.-C. Cheng, G.-Z. Yue, Y.-Q. Wang, G.-L. Kong, J. Appl. Phys. 83 (1998) 7934.
[13] T. Inokuma, Y. Wakayama, T. Muramoto, R. Aoki, Y. Kurata, H. Hasegawa, J. Appl. Phys. 83 (1998) 2228.
[14] A.D. Lan, B.X. Liu, X.D. Bai, J. Appl. Phys. 82 (1997) 5144.
[15] T. Shimizu-Iwayama, Y. Terao, A. Kamiya, M. Takeda, S. Nakao, K. Saitoh, Thin Solid Films 276 (1996) 104.
[16] L.T. Canham, Appl. Phys. Lett. 57 (1990) 1046.
[17] A.J. Read, R.J. Needs, K.J. Nash, L.T. Canham, P.D.J. Calcott, A. Qteish, Phys. Rev. Lett. 69 (1992) 1232.
[18] A.G. Cullis, L.T. Canham, Nature 353 (1991) 335.
[19] G.D. Sanders, Y.-C. Chang, Appl. Phys. Lett. 60 (1992) 2525.
[20] T. Takagahara, K. Takeda, Phys. Rev. B 46 (1992) 15578.
[21] R. Behrensmeier, F. Namavar, G.B. Amisola, F.A. Otter, J.M. Galligan, Appl. Phys. Lett. 62 (1993) 2408.
[22] K.L. Narasimhan, S. Banerjee, A.K. Srivastava, A. Sardesai, Appl. Phys. Lett. 62 (1993) 331.
[23] P.F. Trwoga, A.J. Kenyon, C.W. Pitt, J. Appl. Phys. 83 (1998) 3789.
[24] H. Yorikawa, S. Muramatsu, Appl. Phys. Lett. 71 (1997) 644.
[25] G.C. John, V.A. Singh, Phys. Rev. B 50 (1994) 5329.
[26] V. Ranjan, V.A. Singh, G.C. John, Phys. Rev. B 58 (1998) 1158.
[27] G.C. John, V.A. Singh, Phys. Rev. B 54 (1996) 4416.
[28] Y. Kanemitsu, Phys. Rev. B 53 (1996) 13515.
[29] H. Berthlot, Ann. Chem. Phys. 66 (1962) 110.
[30] C.M. Hurd, J. Phys. C 18 (1985) 6487.
[31] J.C. Vial, A. Bsiesy, F. Gaspard, R. Herino, M. Ligeon, F. Muller, R. Romestain, R.M. Macfarlane, Phys. Rev. B 45 (1992) 14171.
[32] W. Bludau, A. Anton, W. Heinke, J. Appl. Phys. 45 (1974) 1846.
[33] V.A. Singh, G.C. John, in: K.P. Jain (Ed.), Physics of Semiconductor Nanostructures, Narosa Publishing house, London, 1997, p. 186.
[34] J.P. Proot, C. Delerue, G. Allan, Appl. Phys. Lett. 61 (1992) 1948.
[35] B. Delley, E.F. Steigmeier, Appl. Phys. Lett. 67 (1995) 2370.
[36] H.A. Weakliem, D. Redford, J. Appl. Phys. 50 (1979) 1491.
[37] G.D. Cody, in: J.I. Pankove (Ed.), Semiconductors and Semimetals, vol. 21 (Part B), Academic press, 1984, p. 11.

[38] K. Murayama, S. Miyazaki, M. Hirose, Jpn. J. Appl. Phys. 31 (Part 2) (1992) L1358.
[39] Y. Kanemitsu, Phys. Rev. B 49 (1994) 16845.
[40] D. Kovalev, G. Polliski, M. Ben-Chorin, J. Diener, F. Koch, J. Appl. Phys. 80 (1996) 5978.
[41] A. Nakajima, Y. Sugita, K. Kawamura, H. Tomita, N. Yokoyama, J. Appl. Phys. 80 (1996) 4006.
[42] F. Koch, V. Petrova-Koch, T. Muschik, A. Nikolov, V. Gavrilenko, Mat. Res. Soc. Symp. Proc. 283 (1992) 197.
[43] F. Koch, V. Pertrova-Koch, T. Muschik, J. Lumin. 57 (1993) 271.